Biological fingerprint for patient verification using trunk scout views at various scan ranges in computed tomography

Yasuyuki Ueda[1]*, Junji Morishita[2], Shohei Kudomi[3].

1 Department of Medical Physics and Engineering, Area of Medical Imaging Technology and Science, Division of Health Sciences, Graduate School of Medicine, Osaka University

1-7 Yamadaoka, Suita, Osaka 565-0871, Japan

ueda@sahs.med.osaka-u.ac.jp

06-6879-2443

2 Department of Health Sciences, Faculty of Medical Sciences, Kyushu University

3-1-1 Maidashi, Higashi-ku, Fukuoka, Fukuoka 812-8582 Japan

morishita.junji.894@m.kyushu-u.ac.jp

092-642-6673

3 Department of Radiological Technology, Yamaguchi University Hospital

1-1-1 Minamikogushi, Ube, Yamaguchi 755-8505 Japan

kudomi@yamaguchi-u.ac.jp

0836-22-2631

* Corresponding Author

Abstract

Immediate verification of whether a patient being examined is correct is desirable, even if the scan ranges change during different examinations for the same patient. This study proposes an advanced biological fingerprint technique for the rapid and reliable verification of various scan ranges in computed tomography (CT) scans of the torso of the same patient. The method comprises the following steps: geometric correction of different scans, local feature extraction, mismatch elimination, and similarity evaluation. The geometric magnification correction was aligned at the scanner table height in the first two steps, and the local maxima were calculated as the local features. In the third step, local features from the follow-up scout image are matched to those in the corresponding baseline scout image via template matching and outlier elimination via a robust estimator. We evaluated the correspondence rate based on the inlier ratio between corresponding scout images. The ratio of inliers between the baseline and follow-up scout images was assessed as the similarity score. The clinical dataset, including chest, abdomen–pelvis, and chest–abdomen–pelvis scans, included 600 patients (372 men, 68 ± 12 years) who underwent two routine torso CT examinations. The highest area under the receiver operating characteristic curve (AUC) was 0.996, which was sufficient for patient verification. Moreover, the verification results were comparable to the conventional method, which uses scout images in the same scan range. Patient identity verification was achieved before the main scan, even in follow-up torso CT, under different scan ranges.

Keywords

Biological fingerprint, Biometrics, Patient verification, Computed tomography, Scout image

Introduction

Wrong-patient errors can occur during multiple procedures and processes in all health care settings. No individual in the patient's healthcare team is immune to patient misidentification [1-7]. Therefore, positive patient identification is crucial for ensuring patient safety. Notably, in 2020, the "National Patient Safety Goals Effective July 2020 for the Hospital Program" included the following patient identification method: "To improve the accuracy of patient identification, use at least two patient identifiers when providing care, treatment, and services [8]." Although the standard two-patient identifier process can prevent most wrong-patient errors, a new strategy for patient identification should be incorporated to minimize the risk of human error and improve healthcare workflows and utility [9, 10]. The "Healthcare Financial Management Association Educational Report: The value of precise patient identification" also describes "leveraging software tools and biometric solutions for positive patient identification" in addition to "standardizing processes, such as combining the scheduling, registration, and patient identification processes" [11]. Since the late 2010s, biometrics for healthcare applications has been reported [12]. However, performing conventional patient confirmation and biometric identity verification can increase the workloads of healthcare providers. Therefore, biometrics for healthcare, a simple task for various patients, is preferred [4-7]. Several studies have reported biometric applications in radiologic technology [1-3, 13-27] and forensic pathology [28-35].

Although few reports exist on patient identification errors in imaging studies [36], a study based on the findings of a computed tomography (CT) department in a hospital noted six identification errors during a period of 12 months [37]. In routine clinical CT or magnetic resonance (MR) imaging, scout images are first acquired to determine the scan range of the main scan. A scout scan usually depends on the body part being examined; however, in cases where the same body part is scanned, each scout image often has approximately the same scan range. Scout CT/MR images have great potential as biological fingerprints for positive patient identification, and the use of scout image-based biometrics ensures convenience for health care providers and patients [13,14]. However, biological fingerprint techniques using scout torso CT images have certain limitations in clinical applications that require high versatility [14]. For example, the scan range for routine torso scout CT imaging at every instance is not necessarily the chest–abdomen–pelvis; a patient who underwent chest CT might also undergo a scan of other ranges, such as the abdomen–pelvis, at the next follow-up torso CT examination.

This study aimed to (a) develop trunk scout views of different scan ranges, including the chest, abdomen–pelvis, and chest–abdomen–pelvis, to verify that the patients currently being examined are the correct patients before the main scan of the CT examination, and (b) present outcomes after comparing the proposed method to the conventional method [14], which used scout images in the same scan range.

Materials and methods

Subjects

Our institutional review board approved this retrospective observational study. Written informed consent was not required because of the retrospective design of this study. All procedures conducted in this study conformed to the Declaration of Helsinki.

The dataset used in this study was acquired between May 2015 and May 2016. Two scout CT images were randomly obtained from 600 patients who underwent two routine CT scans of the trunk. Patients aged < 20 years, those who had already received intravenous iodinated contrast, those who did not undergo examination in the supine position, and those who did not have both arms raised, were excluded from this study. All scout views in the dataset were acquired using a CT device (SOMATOM Sensation 64, Siemens Medical Solutions, Forchheim, Germany). In addition, to evaluate the effectiveness of the proposed method using different CT devices, scout views of one case each for the same patient examined using a different CT device (SOMATOM Sensation and Definition, Siemens Medical Solutions, Forchheim, Germany) were compared.

Tables 1 and 2 present the patient characteristics and scan parameters, respectively. The trunk scout images of the image dataset evaluated in this study were cropped to the chest, abdomen–pelvis, and chest–abdomen–pelvis for every 100 baselines or follow-up CT examinations of the 600 patient pairs (Table 3). Figure 1 shows the scan ranges of the chest, abdomen–pelvis, and chest–abdomen–pelvis displayed on a scout CT image of the torso.

Methodology

Outline

The proposed method verifies patient identity between scout images with different scan ranges. However, applying the conventional method [14] to these different scan ranges is challenging. Our evaluation model assumed that the baseline scout image was stored on the image-archiving server and that the patient identity was verified to be correct when the scout image was acquired in the follow-up CT scan. Figure 2 presents a flowchart to verify the identity framework of the proposed method. This procedure comprises four major steps: (a) geometric correction of different scans, (b) local feature extraction, (c) mismatch elimination, and (d) similarity evaluation. The proposed method not only utilizes a template-based matching approach but also uses a point set registration to suppress similar changes between different scan ranges. All processing was performed using MATLAB version R2020a (Math Works Inc., 2020) and Python version 3.8.8 (Scotts Valley, CA, USA) with NumPy version 1.19.2 and Scikit-image version 0.18.2. on a Windows 10 computer with a Ryzen 5950X 3.40 - 4.90 GHz (Advanced Micro Devices, Inc., Santa Clara, Calif) central processing unit and 128 GB of random-access memory.

Geometric correction

The proposed method uses the following geometric correction and a previously reported method [14]. Positioning the height of the scanner table higher or lower in the CT gantry would increase or decrease the transverse width of the patient on the scout image owing to magnification effects. Patient magnification was corrected to the height equivalent to the rotational center by linear interpolation of the height of the scanner table. The magnification factor in the transverse direction on the couch at the rotation center was calculated as follows:

$$\alpha = \frac{D_{so}}{D_{so} + TH},$$

where α denotes the magnification factor, D_{so} denotes the distance from the focal spot in the X-ray tube to the rotation center, and TH is the distance from the couch to the rotation center. All scout CT images were processed based on geometric corrections.

Local feature extraction

The detection algorithm [38-40] for N local feature points in the follow-up scout image performs the following two steps: First, the coordinates of the local maxima in the 3 × 3 region were computed within the couch area of the follow-up scout image. The local maxima were subsequently arranged in descending order of amplitude. The first N local maxima coordinates were obtained as the local feature points in the follow-up scout image.

Mismatch elimination

In the proposed method, each feature point correspondence by template matching is further utilized to evaluate the point set similarity using a robust estimator. The template-matching method via normalized cross-correlation [41] was used to calculate the XY coordinates of the baseline scout image corresponding to each template image. The template images were square areas centered on each local feature point in the follow-up scout image. The XY coordinates were used as the local feature points in the baseline scout image. A transformation was implemented to reduce misregistration due to repetition to account for the changes in patient position between the baseline and follow-up CT examinations. In the previously described method [14], the correspondences between the local feature points were determined by considering the round-trip application of template matching between the respective points. However, this method requires all local feature points to be included in the scan range of both baseline and follow-up CT examinations. Hence, detecting different patient pairs with a high number of accidental inliers is concerning, as verified using a large-scale database containing several scan ranges.

We classified all local feature points as inliers or outliers in the proposed method using the random sample consensus (RANSAC) model [42, 43]. All point samples with residuals smaller than the residual threshold, D, were considered inliers. The number of inliers was calculated randomly for each subsample, and the maximum number of inliers K times was used as the number of inliers. D and K indicate the distance threshold between pairs of corresponding feature points on two scout images and the number of random subsamples, respectively. This study applied the affine transformation M-estimator sample consensus (MSAC) algorithm [43], which is a variant of the RANSAC algorithm. The two main parameters that can be tuned by users and significantly affect the performance of the affine transformation MSAC estimator are the distance threshold (D) and the number of random subsamples (K). We determined that K used for MSAC varied from

500 to 3000, and D varied from 1.0 to 3.0. Furthermore, we set various local feature point numbers, N (50–750), for the five template matrix sizes and evaluated the effectiveness of the proposed method compared with that of the previously described method [14].

Similarity evaluation

To measure image similarity, we determined the correspondence rate C using the following equation:

$$\mathrm{C} = \frac{M}{N},$$

where M is the number of inliers, and N is the total number of local feature points. The correspondence rate is a characteristic factor that distinguishes whether a matched patient pair is the same or different. The C values ranged from 0 to 1, with higher rates accepted for the same patient pair.

Performance evaluation

We evaluated the area under the receiver operating characteristic (ROC) curve (AUC) as a performance measure for the proposed method [44]. The ROC curves calculated using the previous [14] and proposed methods were compared using the paired DeLong's test [45, 46]. Statistical significance was set at P <0.05. Statistical analysis was performed using the computing environment R version 4.1.0 (R Development Core Team, 2021) on Windows 10.

Results

The most successful performance of the proposed method achieved an AUC of 0.996 under a distance threshold of 2.0 pixels (Fig. 3a), 2000 random subsamples (Fig. 3b), 12 × 12 template matrix size (Fig. 4a), and 350 local feature points (Fig. 4b). Moreover, the average processing time with these parameter settings was only 400 s in a 1:1 verification of one patient in a dataset comprising 600 patients. Therefore, the processing time required to verify whether a patient is under examination is less than 1 s.

Figure 3 shows the results of the AUC performance for varying distance thresholds (Fig. 3a) and the number of random subsamples (Fig. 3b) between the corresponding pair of feature points on the two scout images. Figure 4 shows the results of the AUC performance using the proposed method (blue line) and the method reported previously [14] (red line) for varying template matrix sizes (Fig. 4a) and numbers of local feature points (Fig. 4b) between the two scout images. The most successful AUC performance using the previously described method was 0.985, with a local feature point of 300 and a template matrix size of 16 × 16, which was consistent with the optimal parameter values reported previously [14]. Figure 5 shows the ROC curves for the most successful performances, with an AUC of 0.996 under the proposed method compared to 0.985 under the previous method [14]. A significant difference was observed between the proposed and previous methods [14] ($P < 0.05$).

Figures 6 and 7 show example images of biological fingerprint analysis using the proposed method (Fig. 6) and the previously described method [14] (Fig. 7). The scan condition of each scout image in both Figures 6 and 7 is as follows: the center (c) is of the baseline examination acquired using a SOMATOM Sensation64, the top-left (a) is of a follow-up examination of the same patient (c) acquired using the same device, the bottom-left (b) is a follow-up examination of the same patient; (c) acquired using a different device (SOMATOM Definition); the top-right (d) is a follow-up examination of a different patient (c) acquired using the same device, and the bottom-right (e) is a follow-up examination of a different patient, and (c) acquired using a different device (SOMATOM Definition). The results of the comparisons shown in Figures 6 and 7 are as follows: the same patient using the same CT device (a–c), the same patient using different CT devices (b to c), different patients using the same CT device (d–c), and different patients using different CT devices (e–c). In Figure 6, which shows representative results of the proposed method, the corresponding rates were 0.266 (93/350) for the a-to-c comparison, 0.200 (70/350) for the b-

to-c comparison, 0.020 (7/350) for the d-to-c comparison, and 0.029 (10/350) for the e-to-c comparison. In Figure 7, which shows the results of the previously described method [14], the corresponding rates were 0.343 (103/300) for the a-to-c comparison, 0.307 (92/300) for the b-to-c comparison, 0.117 (35/300) for the d-to-c comparison, and 0.087 (26/300) for the e-to-c comparison. A comparison of the different CT devices showed a decreased correspondence rate for the previous method [14]; however, the correspondence rate did not change significantly in the proposed method. As shown in Figure 7 (d–c and e–c), the previous method [14] did not sufficiently eliminate the mismatch correspondence, such as mapping between the lungs and pelvis; however, the proposed method did (Fig. 6).

Discussion

This study proposes an advanced biological fingerprint technique using scout CT images of the trunk in a clinical setting. In a previously described method [14], the patient's identity was verified if a scout CT image was obtained in the same range as the previous image during the examination or even in the absence of the patient after the examination. The proposed method makes it possible to verify a patient's identity, even in a frequently occurring clinical situation where the scan range differs from previous examinations. This is beneficial for use in an actual clinical image dataset that contains the stored time-series of scout CT images in a picture archiving and communication system (PACS). In previous studies by Morishita et al. [15], Shimizu et al. [16], and Kao et al. [18], the highest AUCs for patient identity verification using chest X-ray images were 0.993, 0.994, and 0.963 ± 0.002, respectively. Furthermore, Ueda et al. [13] achieved the highest AUC of 0.998 for biometrics based on scout MR brain images. The proposed method yielded the highest verification performance of 0.996 for a template matrix size of 12 × 12, 350 local feature points, a distance threshold of 2.0 pixels, and 2000 random subsamples. The effectiveness of the proposed method was adequate for verifying patient identity in clinical settings and showed a successful performance equivalent to that of the abovementioned methods.

A template matrix size of 4 × 4 (8.0 × 8.0 mm^2 of spatial size) was too small to distinguish each image similarity as a local feature. In addition, if the size of the template matrix exceeds 12 × 12 (24.0 × 24.0 mm^2 of spatial size), positioning reproducibility due to changes in patient posture will affect verification. With the proposed method, the performance improved with increasing numbers of local feature points up to 350 but decreased above that number. Local maxima with peak sizes smaller than the top 350 were considered inappropriate as local features in the proposed method. Usually, a smaller number of random subsamples, K, is preferred because the computational cost of MSAC is approximately linear with respect to K. In this study, the verification performance improved as the number of subsamples increased, reaching a plateau with 2000 subsamples. In addition, in terms of the distance threshold D, decreasing this distance improves the fit by placing a tighter tolerance on the inlier points; however, it does not necessarily improve performance. In this study, the verification performance was slightly altered by varying the distance threshold, reaching a maximum of 2.0 pixels. Hence, the proposed parameters considered that at least 2000 subsampling numbers and a distance threshold of 2.0 are required to calculate an accurate putative solution using MSAC.

The correspondence rate is a characteristic factor for distinguishing between patient pairs that are the same or different. When each correspondence point was correct, all the lines connecting each inlier point were considered parallel. Therefore, a non-parallel line connecting each inlier point represents an incorrect correspondence point. The higher the number of parallel lines connecting each inlier point, the better are the correct acceptance and rejection rates. A comparison of the proposed method (Fig. 6) to the previously described method [14] (Fig. 7) showed more non-parallel lines in the previous method [14]. The results of the comparisons of the scout image (c) to the follow-up scout image (e) using the proposed method (Fig. 6) did not completely allow the elimination of mismatched mapping from the chest to the pelvis. Nevertheless, the number of connecting lines, that is, the correspondence rate, was smaller in the other patients (d, e) than in the same patient (a, b), and each patient verification was accurate. In contrast, the results of the scout image (c) compared to the four follow-up scout images (a, b, d, e) using the previously reported method [14] (Fig. 7) also mapped a part of the chest to the pelvis. Therefore, accurate verification of the correspondence rate of patients (a, b), which is the same as the correspondence rate for another patient (d, e), may be challenging. This indicates that the proposed method is superior to previous methods [14]. This tendency is reflected in the verification performance. The proposed method is a useful approach that can minimize the risk of the wrong patient being scanned during the CT examination as an added value of the scout views of the trunk, which consist of several scan ranges, such as the chest, abdomen–pelvis, and chest–abdomen–pelvis, which are performed during the actual clinical examination. Thus, individual patients can collate medical records while supporting the primary tasks of healthcare providers and patient convenience.

This study has certain limitations. First, the findings cannot be generalized to other populations because this was a single-center study. The dataset for this study was a retrospective analysis, excluding patients < 20 years of age who were still growing and had a short-term follow-up period of 13 months. For example, patients with cancer are likely to lose weight between two scout views performed with longer periods of separation. Consequently, it was impossible to evaluate the effects of long-term changes in physique with growth and age on verification performance in this study. However, as described previously [14], age-related changes in human skeletal structure have negligible effects on scout CT images for patient verification. In most cases, the interval between follow-up CT examinations is much shorter than age-related changes in the human body. In addition, the dataset in this study was evaluated on a single CT device with the

same acquisition parameters. However, the scan range was chest, abdomen–pelvis, or chest–abdomen–pelvis. Different CT devices have different geometric settings, digital values, and image contrasts in the scout CT images. However, we did not evaluate the overall verification performance of the CT devices used in this study.

Second, we consider the single-center retrospective study design as a major limitation. However, as shown in Figure 6, a preliminary study using different CT devices (SOMATOM Sensation and Definition; Siemens Medical Solutions, Forchheim, Germany) showed a correspondence rate of 0.200 for the same patient pair (b–c) and 0.029 for a different patient pair (e–c). Therefore, we believe that the proposed method can be applied to different CT devices from the same manufacturer. However, further research is required to evaluate CT devices manufactured by different manufacturers. Third, selection bias was possible owing to the retrospective design of this study. The method we propose, as well as the previously reported method [14], has the possibility of performance deterioration in patient situations, such as physical abnormalities (such as trauma), attachment of clinical metal devices, and inclusion of a contrasting medium. Future studies are required, including multiple centers and the implementation of prospective designs.

Conclusions

The proposed method, based on the advanced biological fingerprint technique for routine clinical CT imaging of the trunk, provides a valuable solution for preventing patient misidentification, even if the scan range changes in subsequent examinations, thereby reducing the possibility of medical malpractice due to human error.

Acknowledgments

The authors would like to thank Dr. Takayuki Ishida at Osaka University, Japan, for his valuable advice on improving our manuscript and Editage (http://www.editage.com) for editing this manuscript for English language.

Declarations

Conflict of interest

All authors declare that they have no conflict of interest.

Ethics approval

This study was conducted as a retrospective, observational study and approved by the Institutional Review Board of Osaka University (Approval Number:21064).

Funding

This study was supported by JSPS KAKENHI (Grant Numbers JP18K15590 and JP21K15827).

References

1. Morishita J, Ueda Y. New solutions for automated image recognition and identification: challenges to radiologic technology and forensic pathology. Radiol Phys Technol. 2021;14:123-133. https://doi.org/10.1007/s12194-021-00611-9.
2. Morishita J, Katsuragawa S, Kondo K, Doi K. An automated patient recognition method based on an image-matching technique using previous chest radiographs in the picture archiving and communication system environment. Med Phys. 2001;28:1093-7. https://doi.org/10.1118/1.1373403
3. Morishita J, Watanabe H, Katsuragawa S, et al. Investigation of misfiled cases in the PACS environment and a solution to prevent filing errors for chest radiographs. Acad Radiol. 2005;12:97-103. https://doi.org/10.1016/j.acra.2004.11.008.
4. Bittle MJ, Charache P, Wassilchalk DM. Registration-associated patient misidentification in an academic medical center: causes and corrections. Jt Comm J Qual Patient Saf. 2007;33:25-33. https://doi.org/10.1016/S1553-7250(07)33004-3
5. Danaher LA, Howells J, Holmes P, Scally P. Is it possible to eliminate patient identification errors in medical imaging? J Am Coll Radiol. 2011;8:568-574. https://doi.org/10.1016/j.jacr.2011.02.021.
6. Henneman PL, Fisher DL, Henneman EA, Pham TA, Campbell MM, Nathanson BH. Patient identification errors are common in a simulated setting. Ann Emerg Med. 2010;55:503-509. https://doi.org/10.1016/j.annemergmed.2009.11.017.
7. Schulmeister L. Patient misidentification in oncology care. Clin J Oncol Nurs. 2008;12:495-498. https://doi.org/10.1188/08.CJON.495-498.
8. The Joint Commission. National Patient Safety Goals Effective July 2020 for the Hospital Program, 2020. https://www.jointcommission.org/-/media/tjc/documents/standards/national-patient-safety-goals/2020/npsg_chapter_hap_jul2020.pdf. Accessed on Sep 28 2021.
9. Emergency Care Research Institute. Patient identification errors, 2016. https://www.ecri.org/Resources/HIT/Patient%20ID/Patient_Identification_Evidence_Based_Literature_final.pdf. Accessed on Sep 28 2021.

10. Riplinger, L., Piera-Jiménez, J., Dooling, J. P. Patient identification techniques - Approaches, implications, and findings. Yearb Med Inform. 2020;29:81-86. https://doi.org/10.1055/s-0040-1701984.
11. Healthcare Financial Management Association. The Value of Precise Patient Identification, 2016. https://www.imprivata.com/resources/whitepapers/hfma-educational-report-value-precise-patient-identification. Accessed on Sep 28 2021.
12. Waruhari P, Babic A, Nderu L, Were M C. A review of current patient matching techniques. Stud Health Technol Inform, 2017;238: 205–208. https://doi.org/ 10.3233/978-1-61499-781-8-205.
13. Ueda Y, Morishita J, Kudomi S, Ueda K. Usefulness of biological fingerprint in magnetic resonance imaging for patient verification. Med Biol Eng Comput. 2016;54:1341-1351. https://doi.org/10.1007/s11517-015-1380-x.
14. Ueda Y, Morishita J, Hongyo T. Biological fingerprint using scout computed tomographic images for positive patient identification. Med Phys. 2019;46:4600-4609. https://doi.org/10.1002/mp.13779.
15. Morishita J, Katsuragawa S, Sasaki Y, Doi K. Potential usefulness of biological fingerprints in chest radiographs for automated patient recognition and identification. Acad Radiol. 2004;11:309-15. https://doi.org/ 10.1016/s1076-6332(03)00655-x.
16. Shimizu Y, Matsunobu Y, Morishita J. Evaluation of the usefulness of modified biological fingerprints in chest radiographs for patient recognition and identification. Radiol Phys Technol. 2016;9:240-244. https://doi.org/10.1007/s12194-016-0355-4.
17. Shimizu Y, Morishita J. Development of a method of automated extraction of biological fingerprints from chest radiographs as preprocessing of patient recognition and identification. Radiol Phys Technol. 2017;10:376-381. https://doi.org/10.1007/s12194-017-0400-y.
18. Kao EF, Lin WC, Jaw TS, Liu GC, Wu JS, Lee CN. Automated patient identity recognition by analysis of chest radiograph features. Acad Radiol. 2013;20:1024-1031. https://doi.org/10.1016/j.acra.2013.04.006.
19. Shamir L, Ling S, Rahimi S, Ferrucci L, Goldberg IG. Biometric identification using knee X-rays. Int J Biom. 2009;1:365-370. https://doi.org/10.1504/IJBM.2009.024279.

20. Lamb JM, Agazaryan N, Low DA. Automated patient identification and localization error detection using 2-dimensional to 3-dimensional registration of kilovoltage x-ray setup images. Int J Radiat Oncol Biol Phys. 2013;87:390-393. https://doi.org/10.1016/j.ijrobp.2013.05.021.
21. Silverstein E, Snyder M. Implementation of facial recognition with Microsoft Kinect v2 sensor for patient verification. Med Phys. 2017;44:2391-2399. https://doi.org/10.1002/mp.12241
22. Wiant DB, Verchick Q, Gates P, et al. A novel method for radiotherapy patient identification using surface imaging. J Appl Clin Med Phys. 2016;17:271-278. https://doi.org/10.1120/jacmp.v17i2.6066
23. Parks CL, Monson KL. Automated facial recognition of computed tomography-derived facial images: Patient privacy implications. J Digit Imaging. 2017;30:204-214. https://doi.org/10.1007/s10278-016-9932-7
24. Koike-Akino T, Mahajan R, Marks TK, et al. High-accuracy user identification using EEG biometrics. Conf Proc IEEE Eng Med Biol Soc. 2016;2016: 854– 858.
25. Belgacem N, Fournier R, Nait-Ali A, Bereksi-Reguig F. A novel biometric authentication approach using ECG and EMG signals. J Med Eng Technol. 2015;39:226-238. https://doi.org/10.3109/03091902.2015.1021429
26. Toge R, Morishita J, Sasaki Y, Doi K. Computerized image-searching method for finding correct patients for misfiled chest radiographs in a PACS server by use of biological fingerprints. Radiol Phys Technol. 2013;6:437-443. https://doi.org/10.1007/s12194-013-0221-6
27. Sakai Y, Takahashi K, Shimizu Y, Ishibashi E, Kato T, Morishita J. Clinical application of biological fingerprints extracted from averaged chest radiographs and template-matching technique for preventing left-right flipping mistakes in chest radiography. Radiol Phys Technol. 2019;12:216-223. https://doi.org/10.1007/s12194-019-00504-y
28. Morishita J, Ikeda N, Ueda Y, Yoon Y, Tsuji A. Personal identification using radiological technology and advanced digital imaging: Expectations and challenges J Forensic Res 2021;12:472.

29. Ciaffi R, Gibelli D, Cattaneo C. Forensic radiology and personal identification of unidentified bodies: a review. Radiol Med. 2011;116:960-968. https://doi.org/10.1007/s11547-011-0677-6
30. Clemente MA, La Tegola L, Mattera M, Guglielmi G. Forensic radiology: An update. J Belg Soc Radiol. 2017;101:21. https://doi.org/10.5334/jbr-btr.1420
31. Matsunobu Y, Morishita J, Usumoto Y, Okumura M, Ikeda N. Bone comparison identification method based on chest computed tomography imaging. Leg Med (Tokyo). 2017;29:1-5. https://doi.org/10.1016/j.legalmed.2017.08.002
32. Wada Y, Morishita J, Yoon Y, Okumura M, Ikeda N. A simple method for the automatic classification of body parts and detection of implanted metal using postmortem computed tomography scout view. Radiol Phys Technol. 2020;13:378-384. https://doi.org/10.1007/s12194-020-00581-4
33. Kawazoe Y, Morishita J, Matsunobu Y, Okumura M, Shin S, Usumoto Y, Ikeda N. A simple method for semi-automatic readjustment for positioning in post-mortem head computed tomography imaging. Journal of Forensic Radiology and Imaging. 2019;16:57-64. https://doi.org/10.1016/j.jofri.2019.01.004
34. Krishan K, Chatterjee PM, Kanchan T, Kaur S, Baryah N, Singh RK. A review of sex estimation techniques during examination of skeletal remains in forensic anthropology casework. Forensic Sci Int. 2016;261:165.e1-165.e1658. https://doi.org/10.1016/j.forsciint.2016.02.007
35. Tsubaki S, Morishita J, Usumoto Y, et al. Sex determination based on a thoracic vertebra and ribs evaluation using clinical chest radiography. Leg Med (Tokyo). 2017;27:19-24. https://doi.org/10.1016/j.legalmed.2017.06.003
36. Jones DN, Thomas MJ, Mandel CJ, Grimm J, Hannaford N, Schultz TJ, Runciman W. Where failures occur in the imaging care cycle: lessons from the radiology events register. J Am Coll Radiol. 2010;7:593-602. doi: 10.1016/j.jacr.2010.03.013.
37. Barnosky V. Patient identification errors in computed tomography: a plan, do, study, act approach to safety. Radiol Technol. 2014 Jul-Aug;85(6):679CT-681CT.
38. Vincent L, Dougherty ER. Morphological segmentation for textures and particles. In: ER Dougherty, ed. Digital Image Processing Methods. Marcel Dekker: New York 1994;43–102.

39. Krissian K, Carreira J M, Esclarin J, Maynar M. Semi-automatic segmentation and detection of aorta dissection wall in MDCT angiography. Med Image Anal, 2014;18:83–102. https://doi.org/10.1016/j.media.2013.09.004
40. Fu G, Hojjat S A, Colchester A C. Integrating watersheds and critical point analysis for object detection in discrete 2D images. Med Image Anal, 2004;8:177–185. https://doi.org/10.1016/j.media.2004.06.002
41. Briechle K, Hanebeck UD. 2001. "Template matching using fast normalized cross correlation." Proc. SPIE. 4387: 95– 102.
42. Fischler MA, Bolles RC. Random sample consensus: a paradigm for model fitting with applications to image analysis and automated cartography. Commun ACM. 1981;24:381-395. https://doi.org/ 10.1145/358669.358692
43. Torr PHS, Zisserman A. MLESAC: A new robust estimator with application to estimating image geometry. Comp Vis Image Underst. 2000;18:138–156. https://doi.org/10.1006/cviu.1999.0832.
44. International Organization for Standardization. Information technology - Biometric Performance Testing and Reporting - Part 1: Principles and Framework (ISO/IEC 19795-1:2006), 2006.
45. DeLong ER, DeLong DM, Clarke-Pearson DL. Comparing the areas under two or more correlated receiver operating characteristic curves: a nonparametric approach. Biometrics. 1988;44:837-845.
46. Robin X, Turck N, Hainard A, et al. pROC: an open-source package for R and S+ to analyze and compare ROC curves. BMC Bioinform. 2011;12:77. https://doi.org/10.1186/1471-2105-12-77.

Figures

Fig. 1 Example of a trunk scout computed tomography image demonstrating the scan ranges of the chest, abdomen–pelvis, and chest–abdomen–pelvis. The red, blue, and green rectangles indicate the scan ranges of the chest, abdomen–pelvis, and chest–abdomen–pelvis, respectively. The range between the lower chest and upper abdomen, indicated in transparent yellow, was scanned, which is common to all scan ranges.

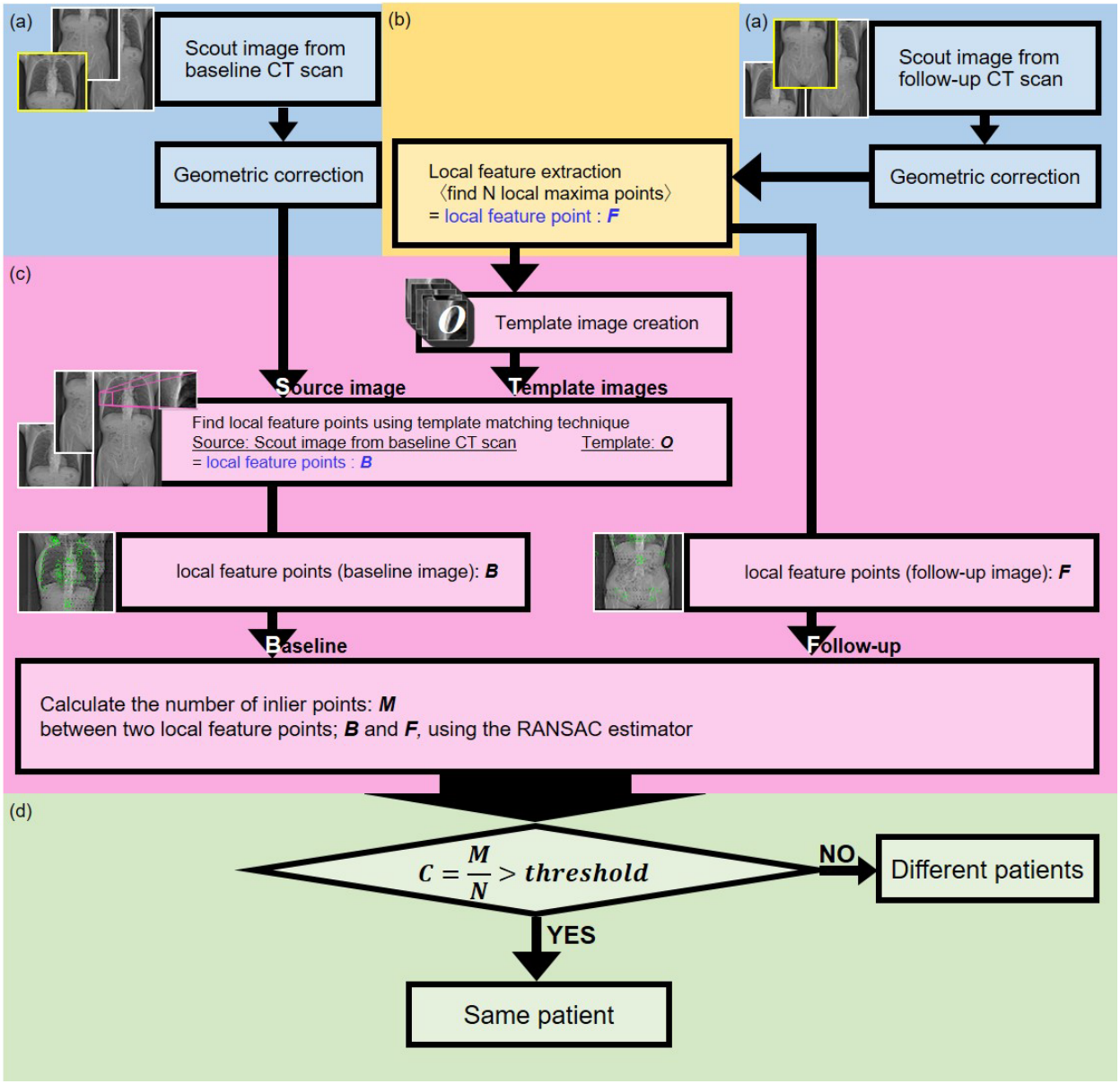

Fig. 2 A flowchart of the proposed biological fingerprint technique framework. The biological fingerprint verification process is performed in four major steps: (a) geometric correction, (b) local feature extraction, (c) mismatch elimination, and (d) similarity evaluation. F: Local feature points in the follow-up computed tomography (CT) image. N: number of local feature points; O: template images. B: local feature points in the baseline scout image. M: number of inlier points. The corresponding rate, C, is a similarity index.

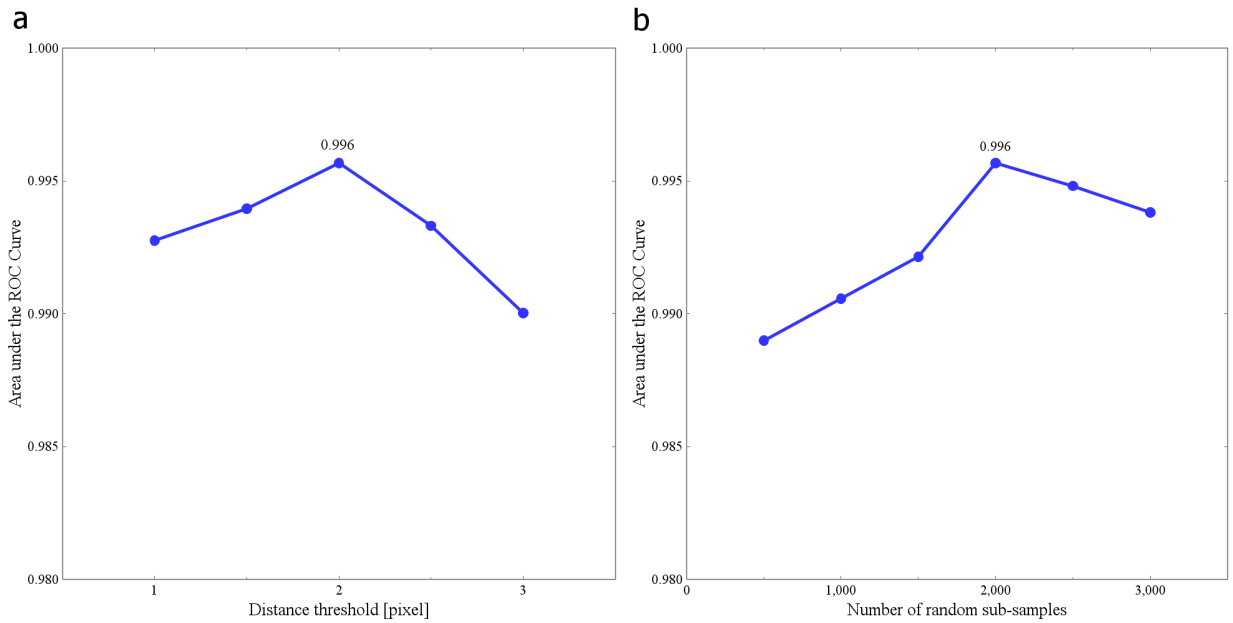

Fig. 3 Quantitative verification performance obtained by two varying parameters using the proposed method in the mixed dataset of the chest, abdomen–pelvis, and chest–abdomen–pelvis scan ranges. (a) Relationships between the distance threshold for the pairs of corresponding feature points on the two scout images and the AUC and (b) the relationships between the number of random subsamples and the AUC. AUC, area under the ROC curve; ROC, receiver operating characteristic.

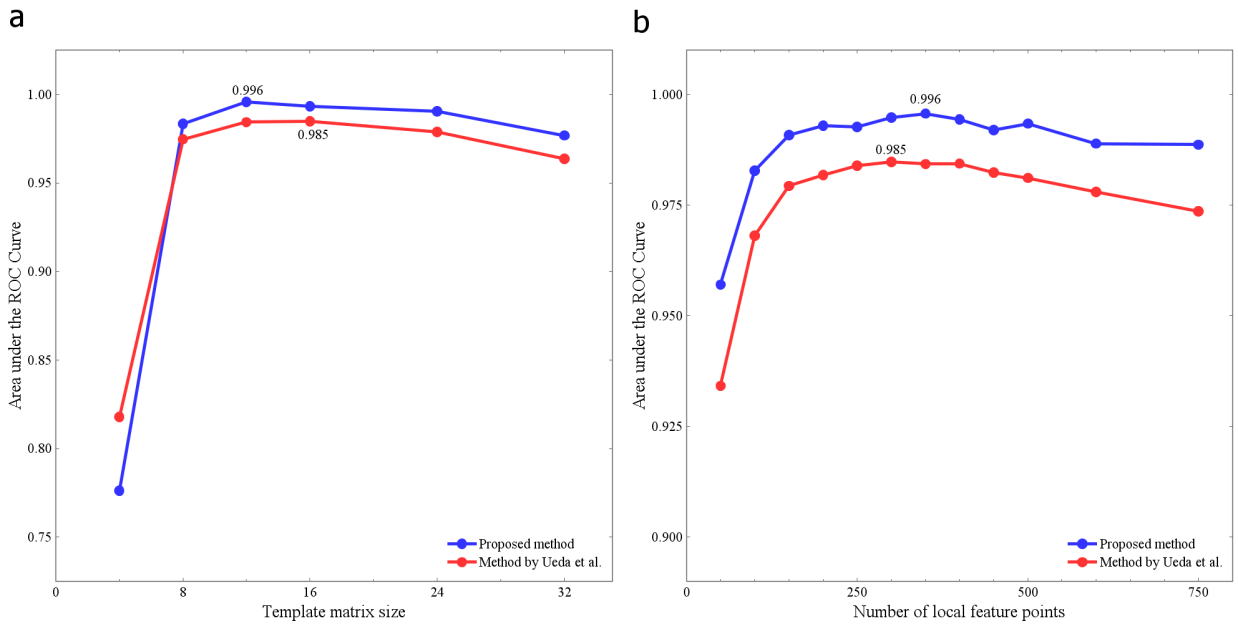

Fig. 4 Quantitative verification performance value obtained by two varying parameters using the proposed method (blue line) and the method by Ueda et al. (14) (red line) in the mixed dataset of the chest, abdomen–pelvis, and chest–abdomen–pelvis scan ranges. The proposed method uses the following parameter settings: D, 2.0 pixels and K, 2000. (a) Relationships between the five template matrix sizes and the AUC. (b) Relationships between the number of local feature points and the AUC. The number of local feature points was 350 for the proposed method and 300 for the previous method. The template matrix sizes were 12 × 12 for the proposed method and 16 × 16 for the method proposed by Ueda et al. (14). D, distance threshold; K, random subsample numbers; AUC, area under the ROC curve; ROC, receiver operating characteristic.

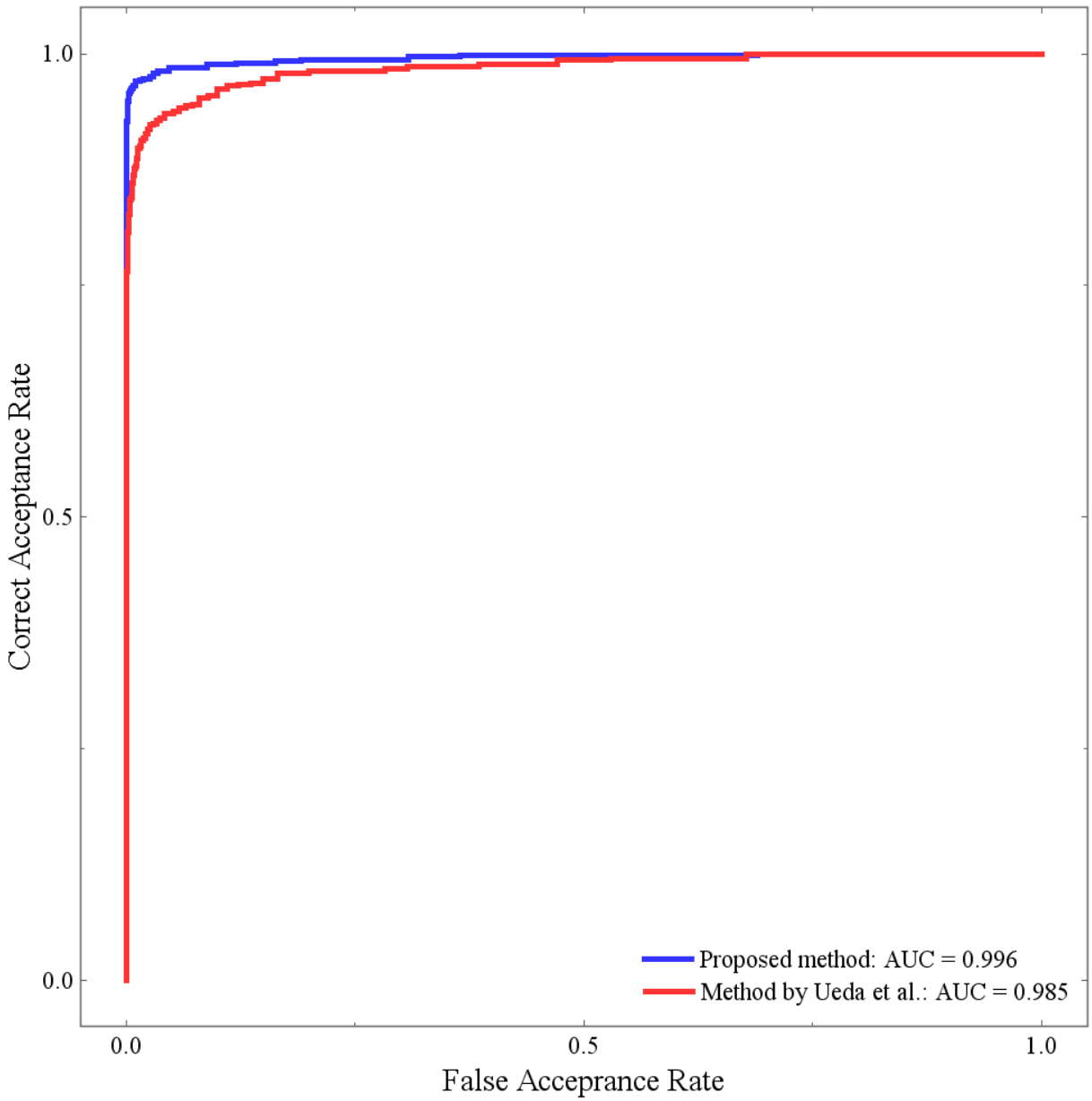

Fig. 5 Comparison of the ROC curves between the proposed method and the method described by Ueda et al. (14) for the parameters that show the maximum AUC. The proposed method (blue line) uses the parameter settings $N = 350$, $X = Y = 12$, $D = 2.0$, and $K = 2000$, with an AUC of 0.996. The method described by Ueda et al. (15) (red line) used the parameter settings $N = 300$ and $X = Y = 16$ and had an AUC of 0.985. The ROC curves differ significantly ($P < 0.05$). *N* number of local feature points; *X* and *Y* rows, and columns of the template matrix size; *D* distance threshold; *K* random subsample numbers; *AUC* area under the ROC curve; *ROC* receiver operating characteristic.

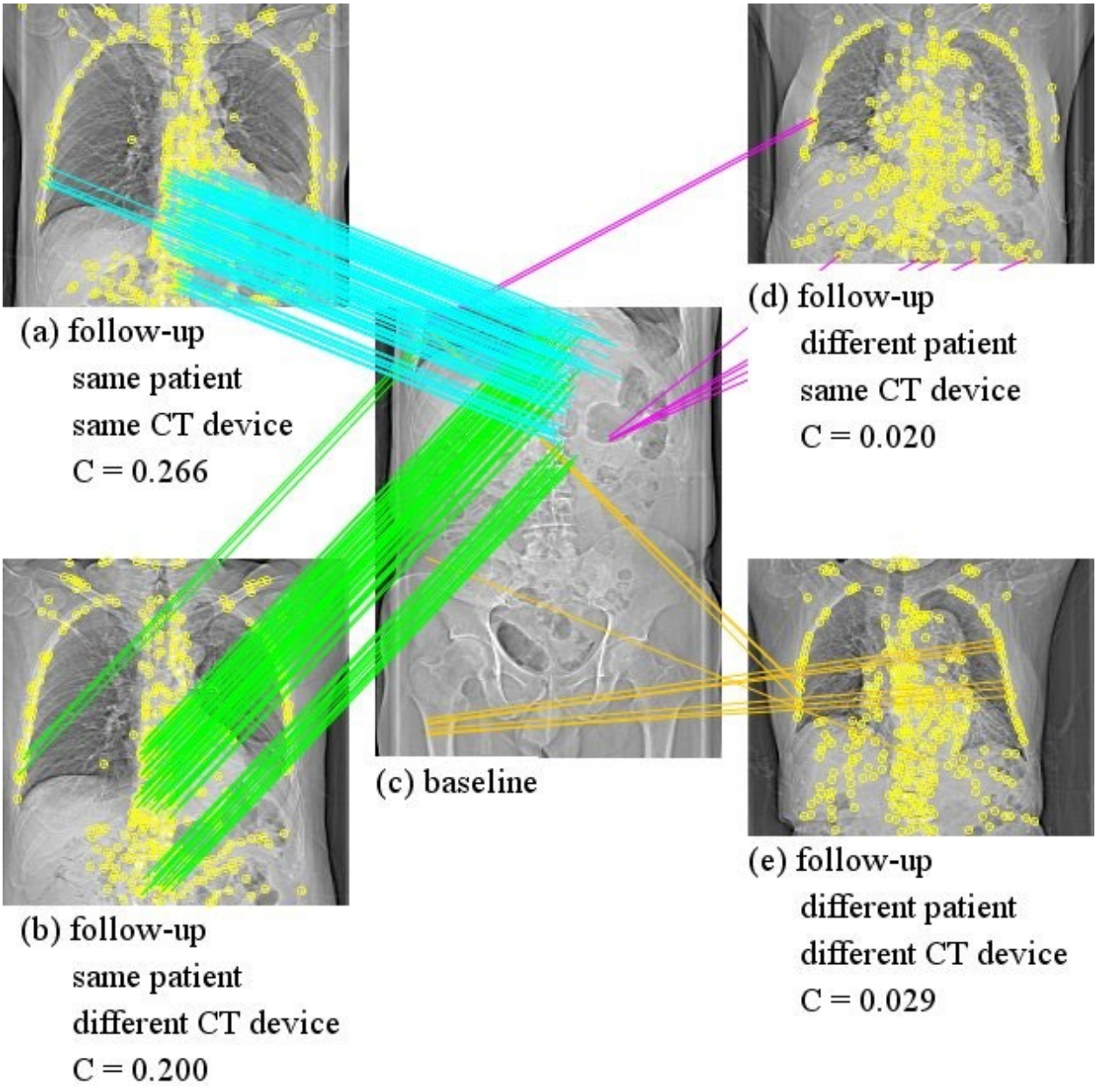

Fig. 6 Example images of the same and different patient-pair analyses with two computed tomography (CT) devices using the proposed method (D = 2.0, K = 2000, X = Y = 12, N = 350). The scan condition of each scout image is as follows: the center (c) is of the baseline examination acquired using a SOMATOM Sensation64 device, the top-left (a) is of a follow-up examination of the same patient (c) acquired using the same device, the bottom-left (b) is of a follow-up examination of the same patient (c) acquired using a different device (SOMATOM Definition), the top-right (d) is a follow-up examination of a different patient (C) acquired using the same device, and the bottom-right (e) is a follow-up examination of a different patient (c) acquired using

a different device (SOMATOM Definition). The yellow circles indicate local feature points. The lines connecting the pairs of yellow circles to the pairs of images are inlier points as follows: the same patient pair acquired using the same CT device (a–c, cyan lines), the same patient pair acquired using a different CT device (b–c, green lines), a different patient pair acquired using the same CT device (d–c, magenta lines), and a different patient pair acquired using a different CT device (e–c, orange lines). The corresponding rates, C, are 0.266 (93/350) for the a-to-c comparison, 0.200 (70/350) for the b-to-c comparison, 0.020 (7/350) for the d-to-c comparison, and 0.029 (10/350) for the e-to-c comparison. *D* distance threshold; *K* number of random subsamples; *X* and *Y* rows and columns of the template matrix size; *N* number of local feature points; *C* correspondence rate.

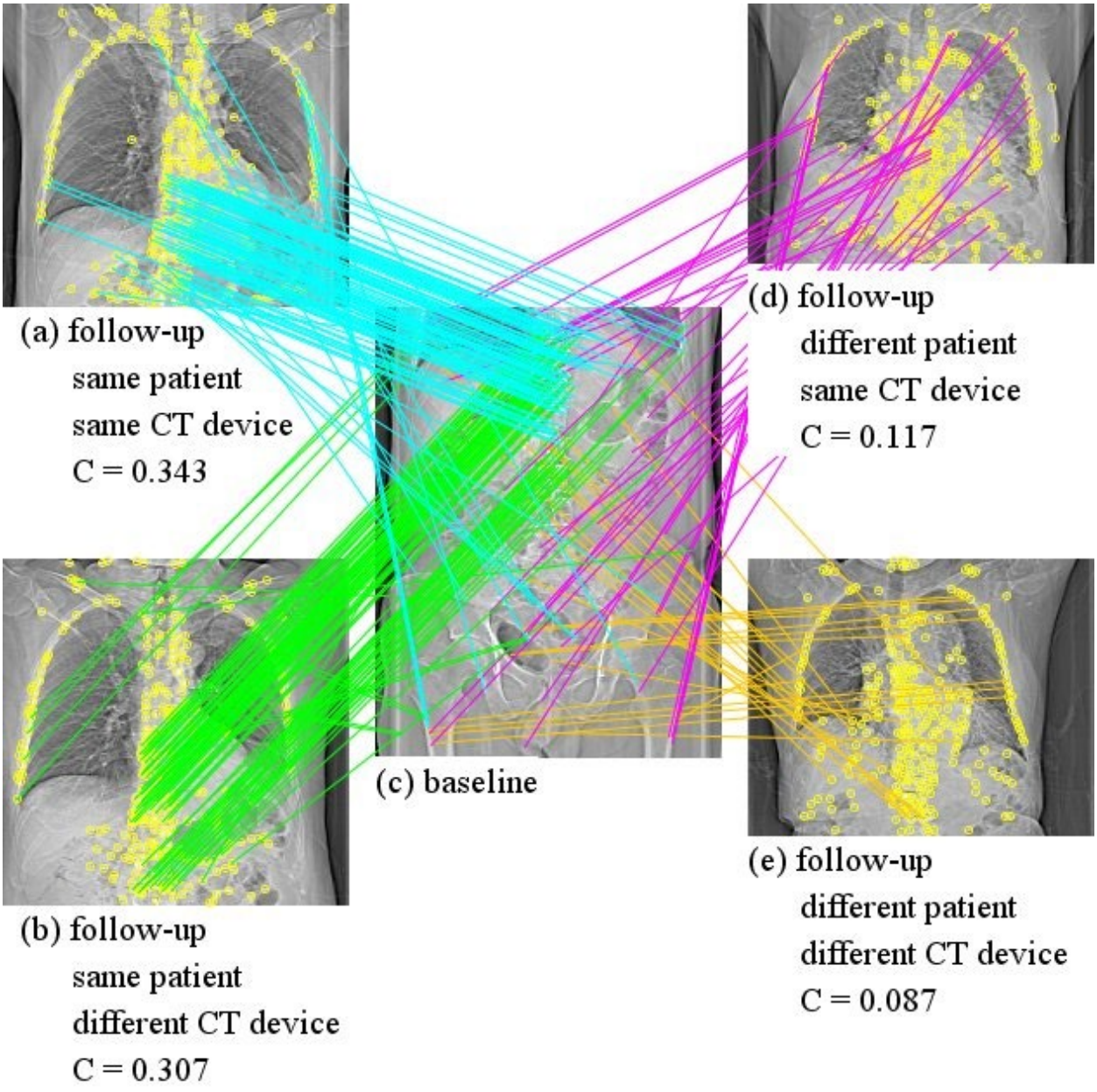

Fig. 7 Example images of the same and different patient-pair analyses with two computed tomography (CT) devices using the method by Ueda et al. (14) (N = 300, X = Y = 16). The scan condition of each scout image is as follows: the center (c) is of the baseline examination acquired using a SOMATOM Sensation64 device, the top-left (a) is of a follow-up examination of the same patient (c) acquired using the same device, the bottom-left (b) is of a follow-up examination of the same patient; (c) is acquired using a different device (SOMATOM Definition); the top-right (d) is a follow-up examination of a different patient (c) acquired using the same device, and the bottom-right (e) is a follow-up examination of a different patient (c) acquired using a different device

(SOMATOM Definition). The yellow circles indicate local feature points. The lines connecting the pairs of yellow circles to the pairs of images are valid corresponding feature points as follows: the same patient pair acquired the same CT device (a–c, cyan lines), the same patient pair acquired using a different CT device (b–c, green lines), a different patient pair acquired using the same CT device (d–c, magenta lines), and a different patient pair acquired using a different CT device (e–c, orange lines).The correspondence rates are 0.343 (103/300) for the a-to-c comparison, 0.307 (92/300) for the b-to-c comparison, 0.117 (35/300) for the d-to-c comparison, and 0.087 (26/300) for the e-to-c comparison. N number of local feature points; X and Y rows, and columns of the template matrix size; C correspondence rate.

Tables

Table 1. Patient characteristics

Number of patients	600
Age	
Mean ± SD (years)	68 ± 12
Range (years)	21–92
Sex	
Male	372
Female	228
Scan intervals	
Mean ± SD (days)	125 ± 75
Range (days)	0-354
Table height	
Mean ± SD (mm)	147 ± 13
Range (mm)	111–209

SD, standard deviation

Table 2. Scan parameters

Tube voltage (kV)	120
Tube current (mA)	35
Physical width of the image measured at the rotation center	
Detector size (mm)	0.6
Field of view (mm)	560

Table 3. Details of the mixed dataset of chest, abdomen–pelvis, and chest–abdomen–pelvis scan ranges

Patient number	Scan ranges	
	Baseline	Follow-up
#1–#100	Chest	Abdomen–pelvis
#101–#200	Chest	Chest–abdomen–pelvis
#201–#300	Abdomen–pelvis	Chest
#301–#400	Abdomen–pelvis	Chest–abdomen–pelvis
#401–#500	Chest–abdomen–pelvis	Chest
#501–#600	Chest–abdomen–pelvis	Abdomen–pelvis